

# Biocompatible, crystalline and amorphous bismuth-based metal-organic frameworks for drug delivery

Claudia Orellana-Tavra,<sup>a</sup> Milan Köppen,<sup>b</sup> Aurelia Li,<sup>a</sup> Norbert Stock<sup>b,\*</sup> and David Fairen-Jimenez<sup>a,\*</sup>

<sup>a</sup>Adsorption & Advanced Materials Laboratory (A<sup>2</sup>ML), Department of Chemical Engineering & Biotechnology, University of Cambridge, Philippa Fawcett Drive, Cambridge CB3 0AS, UK. E-mail: df334@cam.ac.uk.

<sup>b</sup>Institut für Anorganische Chemie, Max-Eyth-Straße 2, D-24118 Kiel, Germany. E-mail: stock@ac.uni-kiel.de.

---

**ABSTRACT:** The synthetic flexibility of metal-organic frameworks (MOFs) with high loading capacities and biocompatibility makes them ideal candidates for drug delivery system (DDS). Here, we report the use of CAU-7, a biocompatible bismuth-based MOF, for the delivery of two cancer drugs, sodium dichloroacetate (DCA) and  $\alpha$ -cyano-4-hydroxycinnamic acid ( $\alpha$ -CHC). We achieved loadings of 33 and 9 wt.% for DCA and  $\alpha$ -CHC, respectively. Interestingly, CAU-7 showed a gradual release of the drugs, achieving time release up to 17 days for DCA and 31 days for  $\alpha$ -CHC. We then performed mechanical and thermal amorphization processes to attempt to delay even more the delivery of guest molecules. With the thermal-treatment, we were able to achieve an outstanding 32% slower release of  $\alpha$ -CHC from the thermal treated CAU-7. Using in vitro studies and endocytosis inhibitors, confocal microscopy and fluorescence-activated cell sorting (FACS), we also demonstrated that CAU-7 was successfully internalized by cancer cells, partially avoiding lysosome degradation. Finally, we showed that CAU-7 loaded either with DCA or  $\alpha$ -CHC had a higher therapeutic efficiency compared with the free drug approach, making CAU-7 a great option for biomedical application.

Key words: MOFs, drug delivery, cancer, controlled release, endocytosis

---

## INTRODUCTION

Conventional pharmaceutical formulations are characterized by a number of drawbacks such as drug-limited solubility, drug degradation before reaching the desired organ, lack of selectivity, poor distribution, and undesired pharmacokinetics.<sup>1-3</sup> Very often, free drugs need to circulate in the blood stream at high concentrations in order to reach a specific organ or tissue at the desired concentration, and this condition may generate healthy tissue damage. By using a drug delivery systems (DDSs), it is possible to overcome the side effects of free drugs,<sup>1,2</sup> achieving a controlled release, improving drug solubility issues, conferring protection from degradation and accomplishing, potentially, a targeted delivery.<sup>4-6</sup>

In the last years, metal-organic frameworks (MOFs) have been widely studied for drug delivery and biosensing applications.<sup>7,8</sup> MOFs are hybrid ordered porous materials made from metal centers connected through organic linkers, offering exceptionally high apparent surface areas (up to 8,000 m<sup>2</sup>/g).<sup>9,10</sup> One of the main advantages of MOFs over organic (e.g. liposomes, micelles) and inorganic (e.g. zeolites, mesoporous silica) systems is their high loading capacities, with values as high as 2 g of

drug per g of solid.<sup>11</sup> In addition, MOF synthetic flexibility offers the possibility for tuning their pore properties and adsorption performance by changing the individual building blocks, i.e. the metal clusters and organic linkers that conform them, to provide the desired properties.<sup>11,12</sup> The almost infinite possible combinations for designing new MOFs with different chemical properties, topologies, pore sizes and shapes,<sup>8,9,12,13</sup> has allowed an amazing growth in this field, with more than 90,000 different structures reported so far.<sup>14-17</sup>

When proposing MOFs for biomedical applications, they require high biocompatibility and low accumulation in cells. The vast number of MOFs allows one to select optimal building blocks, including metals. This includes not only an optimal MOF-drug interaction and loading capacity, but also biocompatible building blocks, as well as an adequate particle size and external surface chemistry that allows a more efficient endocytosis process.<sup>18,19</sup> In the past, one of the most critical limitations in the applicability of MOFs in industry has been the general lack of long-term chemical stability. However, in biomedical applications and specifically in drug delivery, their moderately low aqueous stability is beneficial, so MOF particles can be biodegraded and eliminated from the body after the

drug is released, preventing detrimental accumulation in vivo. Eventually, biocompatible MOFs offer high loading capacities, controlled drug-release, can overcome drug solubility issues and can confer drug protection from degradation.<sup>4-6</sup> In the past years, Horcajada and co-workers pioneered these studies working on the loading of diverse anticancer agents and also investigated the potential of post-synthetic modifications for improving their biological properties.<sup>20-24</sup> Morris and co-workers have greatly contributed in the topical formulation using MOFs, focused on the delivery of nitric oxide (NO) for its use as antithrombotic agent.<sup>25</sup> Mirkin and co-workers reported the first covalently functionalized MOF-oligonucleotide (DNA) conjugated oriented to facilitate the cellular uptake,<sup>26</sup> whereas Wang and co-workers worked on the delivery of DNazymes, single-stranded DNA molecules known as potent therapeutic agents for gene therapy, achieving an efficient delivery without degradation into cancer cells.<sup>27</sup>

Despite the success of MOFs, their relatively poor chemical stability of the MOF family jeopardies many of their advantages for industrial applications. Such chemical instability can be considered advantageous in drug delivery processes, since, unlike e.g. mesoporous silicas, MOF DDS can be easily biodegraded in the body after the drug has been released. One of their principal current limitations as DDS is the fast kinetic drug release during the desorption process – typically below 48 h.<sup>20</sup> We addressed this problem through different strategies: using a post-loading mechanical amorphization, and observing a sustained drug release of more than 30 days;<sup>28</sup> enhancing the therapeutic effect of a cancer drug using large-pore MOFs;<sup>29</sup> as well as using a polyethylene glycol coating, releasing only ca. 40% of the cargo after 5 days, while keeping the remaining amount encapsulated inside the MOF.<sup>30</sup> To the best of our knowledge, such extremely long release times have not been reported before for any MOF or DDS with similar characteristics. For instance, it has been possible to extend the release time of a water-soluble drug up to 5 days using a core-shell microsphere and core-shell biodegradable microfibers with a diameter of ca. 400  $\mu\text{m}$ .<sup>31,32</sup> Also, hydrogel microspheres of 3–5  $\mu\text{m}$  of diameter showed release time prolonged for 13 days. However, when using larger hydrogel cylinders, drug release was increased up to 200 days.<sup>33</sup> All these systems are useful options only in the case of cell membrane permeable drugs and non-parenteral routes of administration. This is because, in contrast with our proposed  $a_m$ MOF system, the size of the carriers is not small enough (i.e.  $\sim 200$  nm) to be endocytosed by cells or to circulate through the smallest capillaries.

In addition to the wealth of different cargoes and tuning possibilities that MOFs offer, understanding the cellular uptake mechanisms for them is a critical aspect in

drug delivery. We recently investigated the role of the particle size<sup>19</sup> and surface chemistry<sup>18,30</sup> on the internalization pathways and intracellular final fate of Zr-based MOFs, eventually allowing to change the efficacy of the MOFs as DDSs. Three endocytic pathways are the most common: clathrin- and caveolae-mediated endocytosis and macropinocytosis.<sup>34,35</sup> Particles internalized through endocytosis enter cells entrapped in vesicles called endosomes. Endosomes formed by clathrin-mediated endocytosis and macropinocytosis become mature vesicles or late endosomes that fuse with lysosomes, leading to the degradation of the drug delivery system and the loaded cargo, consequently diminishing or totally voiding its therapeutic effect.<sup>36</sup> On the other hand, particles internalized via caveolae-mediated endocytosis can later be transported to diverse location in cells. Interestingly, these particles can be delivered to a final intracellular location avoiding the lysosomal degradation.<sup>37-39</sup> eventually, to comprehensively design efficient DDS based on MOFs, it is important to not only have biocompatible systems, but also have a system able to avoid the lysosomal degradation.

In this work, we studied a bismuth-based MOF, CAU-7<sup>40</sup> ([Bi(BTB)]), with  $\text{BTB}^{3-} = 1,3,5$ -benzenetrisbenzoate and CAU standing for Christian-Albrechts-Universität), as a DDS. Despite the fact that bismuth presents low toxicity – being used broadly in medicine and veterinary practice<sup>41,42</sup> – to the best of our knowledge, no previous studies have used it for drug delivery. We loaded CAU-7 with the cancer drugs sodium dichloroacetate (DCA) and  $\alpha$ -cyano-4-hydroxycinnamic acid ( $\alpha$ -CHC), both capable of modifying cancer metabolic pathways.<sup>43-46</sup> DCA is involved in restoring the normal metabolic respiration in the mitochondria – lost in cancer cells – and therefore inducing apoptosis.<sup>47</sup> The abnormal glucose metabolism and reduced mitochondrial oxidation of tumor cells is indeed an enormous advantage for them as it contributes to tumor growth independently of the oxygen present.<sup>48</sup> On the other hand,  $\alpha$ -CHC has the ability to inhibit the protein monocarboxylate transporter 1 (MCT1), upregulated in diverse types of cancer.<sup>45,49</sup> We used a complete combination of in vitro studies, confocal microscopy, fluorescence-activated cell sorting (FACS) and Monte Carlo simulations to confirm the successful incorporation of CAU-7 into the cells and to understand the cellular uptake mechanism for CAU-7 internalization.

## RESULTS AND DISCUSSION

### STABILITY AND BIOCOMPATIBILITY OF CAU-7

CAU-7 forms trigonal prismatic particles and the framework structure is composed of  $\text{Bi}^{3+}$  ions and  $\text{BTB}^{3-}$  linker molecules ( $\text{BTB}^{3-} = 1,3,5$ -benzenetrisbenzoate); the  $\text{Bi}^{3+}$  ions are nine-fold coordinated by oxygen atoms of the  $\text{BTB}^{3-}$  ions (Figure S1). The  $\text{BTB}^{3-}$  linker molecules build

the wall of a honeycomb network with approximately 10 Å wide and one-dimensional channels ( $S_{\text{BET}} = 1150 \text{ m}^2\text{g}^{-1}$ ,  $V_p = 0.43 \text{ cm}^3\text{g}^{-1}$ ).<sup>40</sup> We selected a bismuth-based MOF due to its biocompatibility, already established in the medicinal and cosmetic chemistry. For example, the well-known bismuth-based Pepto-Bismol™ (bismuth subsalicylate) is widely used for stomach disorders,<sup>50</sup> bismuth oxychloride is used in personal care products and bismuth nitrate is used as an antiseptic during surgery.<sup>50</sup> The lethal dose ( $\text{LD}_{50}$ ) of bismuth oxychloride ( $\text{BiOCl}$ ), 22 g/kg (rat, oral), and bismuth oxide, 10 g/kg (mouse, oral), are rather high compared to other metals.<sup>51</sup>

Figure S2 provides the powder X-ray diffraction (PXRD) data of CAU-7, confirming the phase purity of the reaction product;  $\text{N}_2$  adsorption isotherms confirmed the porosity of nanocrystalline CAU-7 (Figure S3). Figure S4 shows the scanning electron microscopy (SEM) images of the sample, indicating the heterogeneous particle size of the MOF, with particle size of around  $195 \pm 12 \text{ nm}$  and  $477 \pm 40 \text{ nm}$ . Since the tendency of particle aggregation is determined by the surrounding media,<sup>52</sup> we used dynamic light scattering (DLS) to measure the hydrodynamic diameter (HD) of CAU-7 in growth media and phosphate-buffered saline (PBS). Interestingly, the degree of aggregation was higher when the MOF particles were suspended in PBS ( $\text{HD} = 10,439 \pm 1672 \text{ nm}$ ) compared to growth media ( $\text{HD} = 205 \pm 3 \text{ nm}$ ). Arguably, a protein corona formed around the CAU-7 particles through the adsorption of growth media proteins on the external surfaces able to improve its water stability. We analyzed the degradation profile of CAU-7 by incubating it in PBS and water. **Figure 1** shows the release of the organic linker, the powder X-ray diffraction (PXRD) patterns and the FTIR profiles, demonstrating the higher stability of CAU-7 in water compared to PBS. After 13 days, CAU-7 released ca. 56% and 5% of the linker in PBS and water, respectively, whereas 2 days of incubation in PBS is enough to make CAU-7 completely amorphous (**Figure 1b**). After incubation in PBS, an intense band at around  $1000 \text{ cm}^{-1}$ , corresponding to  $\text{PO}_4^{3-}$ , appeared, while the peaks attributed to  $\text{BTB}^{3-}$  decreased dramatically (band at  $1690 \text{ cm}^{-1}$  assigned to the C=O stretching vibration of aromatic carboxylic acids and band ranging from  $1605 - 1507 \text{ cm}^{-1}$  assigned to C-H and ring C-C stretching vibrations), confirming the exchange of the linker by the phosphate (**Figure 1c**). Since phosphate salts are a common electrolyte in the human body, one can expect that CAU-7 will degrade in vivo and will avoid intracellular accumulation and toxicity. Similar degradation effect of PBS has been seen before for Zr-based MOFs such as UiO-66.<sup>53</sup>

Following the degradation studies, we measured the in vitro cytotoxicity of CAU-7 and building blocks on HeLa cells. **Figure 2** shows the MTS viability values for CAU-7,

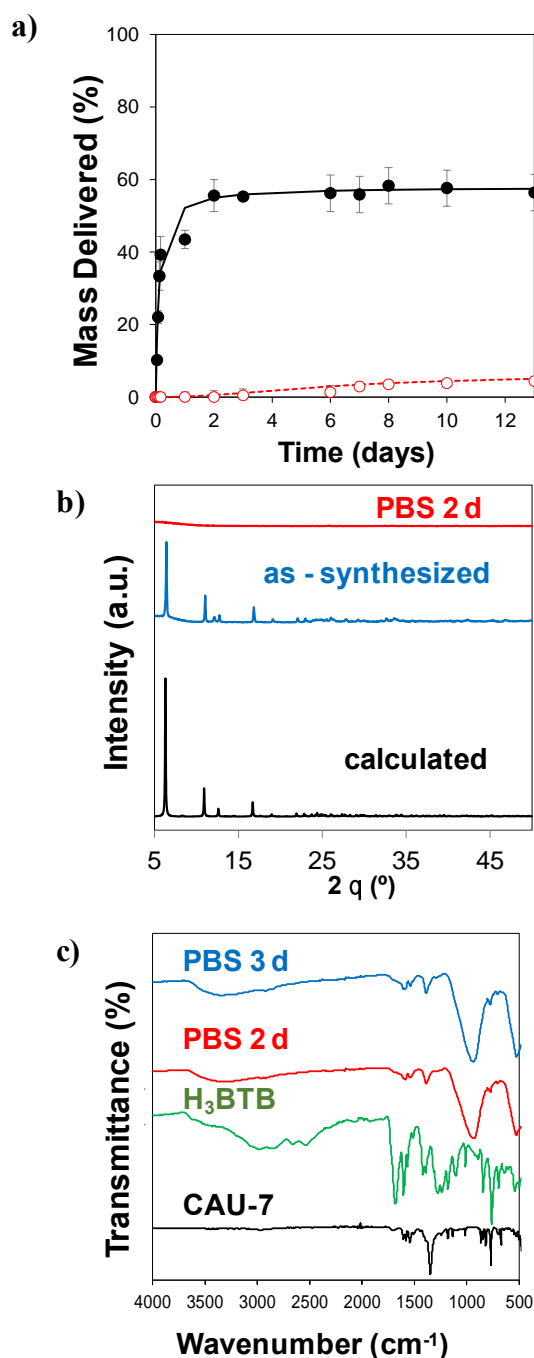


**Figure 1.** Stability analysis for CAU-7. **a.** Degradation pattern in PBS (black closed dots) and  $\text{H}_2\text{O}$  (red open dots). **b.** PXRD patterns of calculated CAU-7 (black), as-synthesized (blue) and samples incubated for 2 days in PBS (red). **c.** FTIR analysis after PBS exposure for 0 days (black), 2 days (red) and 3 days (blue) and  $\text{H}_3\text{BTB}$  (green).

$\text{H}_3\text{BTB}$  and the bismuth salt  $\text{Bi}(\text{NO}_3)_3$ . The MOF and components are biocompatible in the range analyzed, as none of the used concentrations exhibited a significant difference compared to untreated cells.

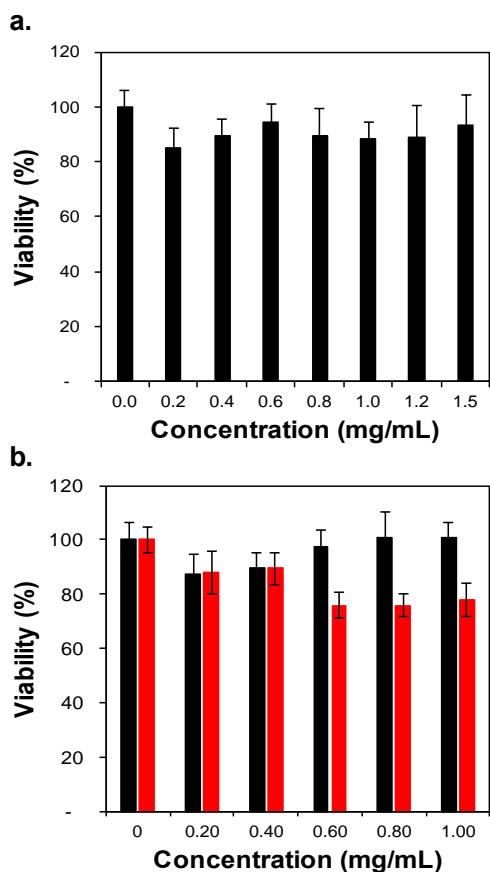


**Figure 2.** MTS viability assay after 24h on HeLa cells for: **a.** CAU-7, **b.** H<sub>3</sub>BTB (black bars) and Bi(NO<sub>3</sub>)<sub>3</sub> (red bars). The error bars represent the standard combined error of three independent samples.

## DRUG ADSORPTION AND ENCAPSULATION ON CRYSTALLINE AND AMORPHOUS CAU-7

After loading DCA and  $\alpha$ -CHC into CAU-7 (33.7 and 9.3 wt.% for DCA and  $\alpha$ -CHC, respectively), we confirmed, using PXRD, that CAU-7 was able to retain its crystalline structure (Figure S5). We also performed Monte Carlo simulations to better understand the adsorption of DCA and  $\alpha$ -CHC in CAU-7. The maximum capacities were predicted to be 33.3 wt.% (10.1 mol of drug/mol of CAU-7) and 19.9 wt.% (13.7 mol of drug/mol of CAU-7) for DCA and  $\alpha$ -CHC, respectively, whereas the experimental maximum loadings we obtained were of 33.7 wt.% (9.8 mol of DCA/mol of CAU-7) and 9.3 wt.% (33.2 mol of  $\alpha$ -CHC/mol of CAU-7). Looking at the sizes of both drugs, it is clear that DCA was able to diffuse through the pores whereas  $\alpha$ -CHC showed some issues getting loaded. The data also suggests there is space for improvement. **Figure 3** shows snapshots of the adsorption process of these two drugs by CAU-7 at low, medium and saturated loadings; **Figure S6** shows the density distributions during the adsorption process, highlighting the areas where the molecules get adsorbed. DCA and  $\alpha$ -CHC are first adsorbed

on the walls of the MOF structure at low loadings, before filling up the whole cavity at higher loadings.

**Figure 4** shows the experimental delivery profiles for DCA and  $\alpha$ -CHC from CAU-7, exhibiting a two-stage release (Table S6 shows the fitted equations). In the case of DCA, 75% of the release takes place in the first 4 h, whereas total release is accomplished at 17 days. A similar but slightly slower process is obtained for  $\alpha$ -CHC, with 65% released in the first 5 h, and total release at 31 days. The first stage of delivery might be associated with desorption of drug molecules weakly adsorbed in center of the large pores of CAU-7, as found using GCMC simulations, whereas the second stage may be related with desorption of molecules with a stronger interaction with the pores of CAU-7.

At this point, we then attempted to slow down the release of the drugs from CAU-7 by inducing an encapsulation of the guest drugs through an amorphization process. In the first place, we used a ball-milling, mechanical amorphization process on the loaded CAU-7, generating the  $a_m$ CAU-7 sample.<sup>28,54</sup> Separately, we performed a temperature based amorphization, generating the  $a_t$ CAU-7 sample, where the fast removal of the solvent from the pores provokes the collapse of the framework by the action of the internal forces in the liquid-gas meniscus.<sup>55</sup> Indeed, MOFs possessing large pores have been found particularly susceptible to these issues, presenting discrepancies between the estimated and experimental surface areas after activation.<sup>56</sup> However, from a different point of view, solvent removal may be a powerful and useful alternative in order to develop amorphous materials by inducing a framework collapse. PXRD confirms the partial structural degradation of both  $a_m$ CAU-7 and  $a_t$ CAU-7 (Figure S5).

The drug release profiles differ for both drugs and mechanical/temperature amorphization processes. For DCA,  $a_m$ CAU-7 reproduces the profile of crystalline CAU-7, with a small decrease in the total amount released, whereas  $a_t$ CAU-7 releases DCA much faster, with a single-step hyperbolic curve and total release at 4 days (see Tables S6-S7 for fitting equations). The fast release is probably triggered by water molecules dragging DCA from the pores during the thermal treatment, possibly due to the high loading levels of DCA in the MOF (33 wt.%) and its small size and high affinity to water. In the case of  $\alpha$ -CHC, both  $a_m$ CAU-7 and  $a_t$ CAU-7 follow the same profile of crystalline CAU-7, but the release was significantly slower, in particular for  $a_t$ CAU-7; between days0 and 4, the difference in the amount released was 32% lower from  $a_t$ CAU-7 and 19% for  $a_m$ CAU-7 both compared to crystalline-CAU-7. The slower release from  $a_m$ CAU-7 and  $a_t$ CAU-7 would be related to the slow dissolution of the amorphous frameworks.

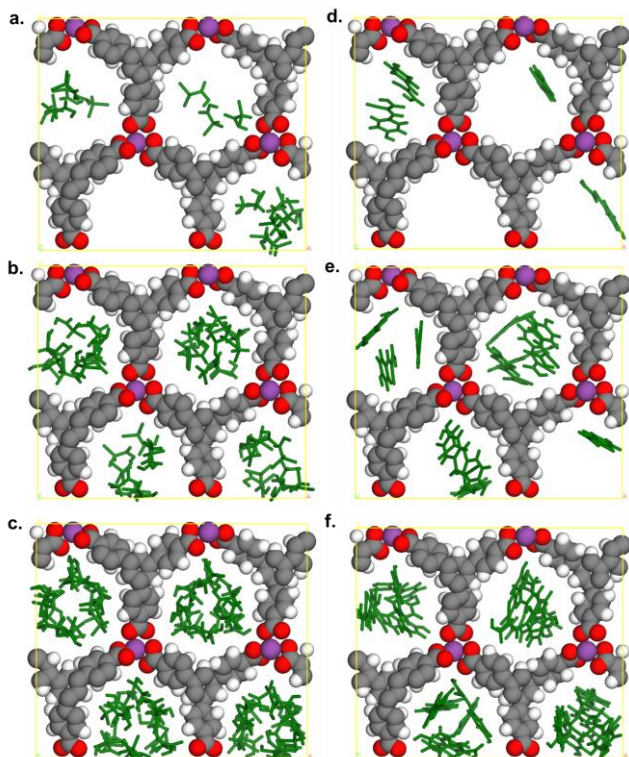


**Figure 3.** Snapshots of DCA (a. to c.) and  $\alpha$ -CHC (d. to f.) in CAU-7 at different loadings: a. 121  $\text{mg.g}^{-1}$  or 10.8 wt.%, b. 307  $\text{mg.g}^{-1}$  or 23.5 wt.%, c. saturation with 500  $\text{mg.g}^{-1}$  or 33.3 wt.%, d. 42  $\text{mg.g}^{-1}$  or 4.0 wt.%, e. 126  $\text{mg.g}^{-1}$  or 11.2 wt.% and f. saturation with 248  $\text{mg.g}^{-1}$  or 19.9 wt.%. The drug molecules are represented in green-stick mode.

### IN VITRO PERFORMANCE OF CAU-7

To study the performance of CAU-7 as a DDS for cancer, we first confirmed its ability to be internalized by cells. **Figure 5** shows the confocal microscopy images of HeLa cells incubated for 24 h with a CAU-7 sample loaded with the hydrophilic and fluorescent molecule calcein (cal@CAU-7) as well as with free calcein. Similar to previous studies, cells treated with only free calcein stained weakly and in the form of bright vesicles after 24 h, suggesting the entrapment of dye in endosomes.<sup>19,28</sup> On the other hand, when using cal@CAU-7 the fluorescent signal was significantly stronger. The images are an internal plane of cells, allowing the simultaneous visualization of the nucleus (blue), cal@CAU-7 (green) and cell membrane (red). All this confirms that CAU-7 was effectively inside the cells and not attached to the exterior cell membrane.

We followed the confocal imaging of CAU-7 by investigating the endocytic pathways used by HeLa cells in order to fully understand their internalization and final fate. Indeed, the chosen pathway may determine the possible escape from lysosomal degradation, making the DDS a more efficient system. We used sucrose and chlorpromazine endocytosis inhibitors to block clathrin-mediated en-

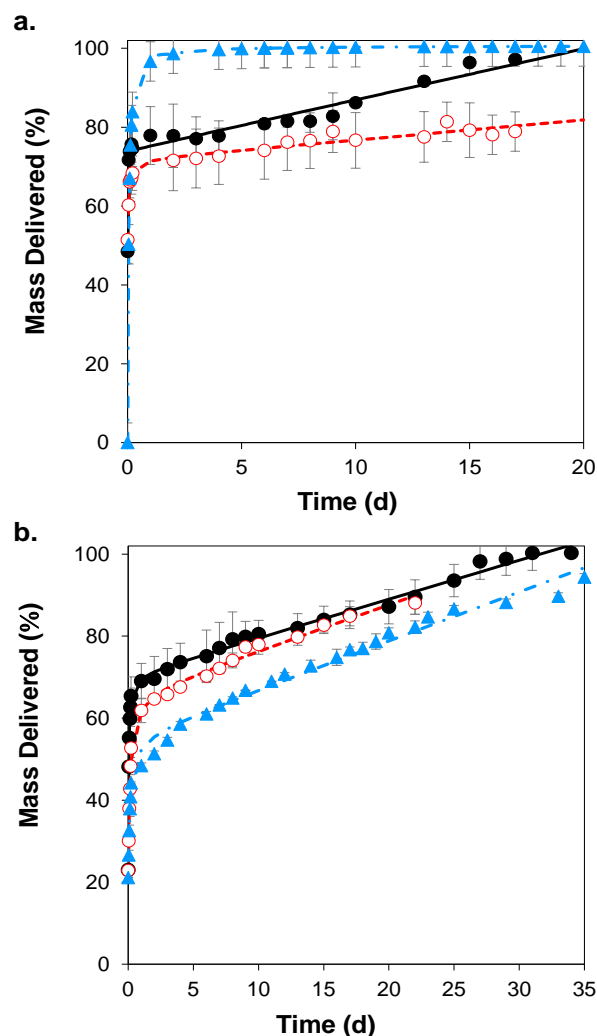


**Figure 4.** Release profile of a. DCA and b.  $\alpha$ -CHC, from crystalline CAU-7 (black closed circles), mechanically amorphous  $a_m$ CAU-7 (red opened circles), and thermally amorphous  $a_t$ CAU-7 (blue closed triangles). Black solid, red dotted and blue dotted lines represent the kinetic of delivery fitting using non-linear regression on crystalline, mechanically amorphous and thermally amorphous materials, respectively.

docytosis, nystatin to inhibit caveolae-mediated endocytosis and rottlerin to inhibit macropinocytosis. Figure 6 presents the normalized internal fluorescence, using Flowcytometry assays (FACS), of HeLa cells after incubation with the different endocytosis inhibitors. The internalization of CAU-7 was highly inhibited down to 18% after incubation at 4 °C compared to the control at 37 °C, confirming that the uptake of CAU-7 occurs through an energy dependent process – endocytosis – rather than simple diffusion.<sup>36,57,58</sup> CAU-7 uptake was also strongly inhibited when cells were incubated together with sucrose and chlorpromazine, reaching levels of 23 and 47%, respectively. This indicates that both inhibitors affected differently the clathrin-mediated pathway. Despite sucrose

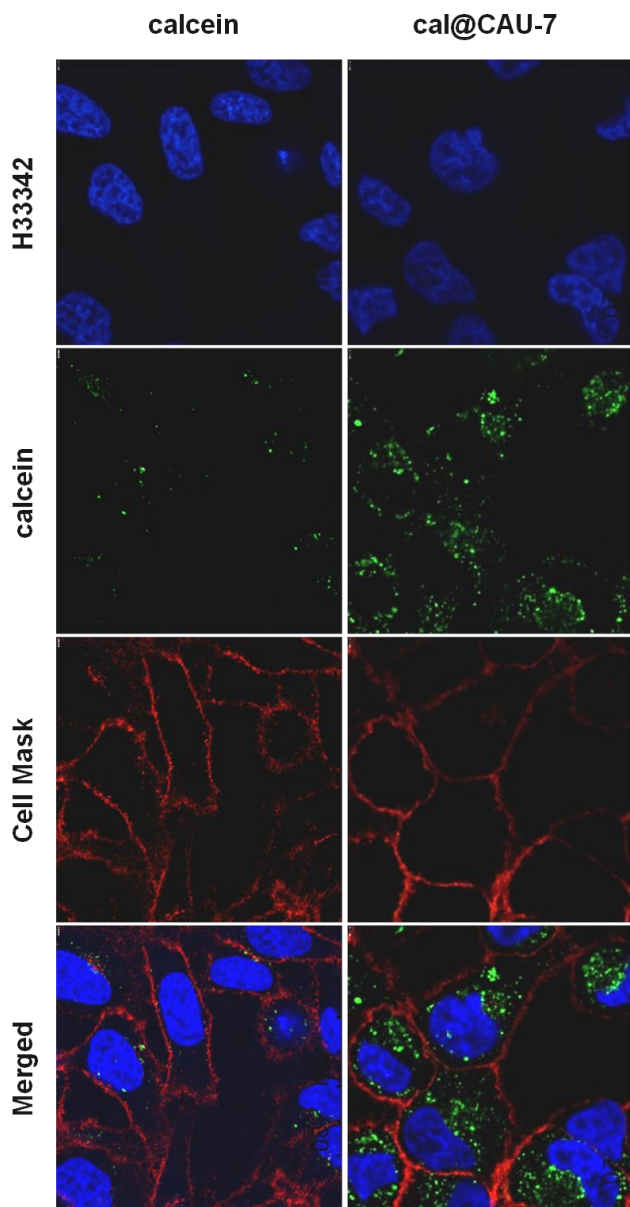


**Figure 5.** Confocal microscopy images of HeLa cells incubated with cal@CAU-7 or free calcein for 24 h.

being considered an inhibitor of clathrin-mediated endocytosis, there is some evidence that it can affect non-clathrin-mediated pathways as well.<sup>59</sup> For this reason, we used chlorpromazine to confirm the result since there is no evidence that it affects caveolae-mediated endocytosis or any other pathways.<sup>36</sup> On the other hand, when using nystatin, internalization levels reduced to 58%; no statistical difference was found when treated with rottlerin. This result indicates that the trafficking of CAU-7 is made mainly through clathrin- and caveolae-mediated endocytosis, whereas macropinocytosis has a minor effect. Importantly, for particles undergoing caveolae-mediated endocytosis it may be possible to partially avoid the lysosome compartment and their further degradation – something critical for DDS design.

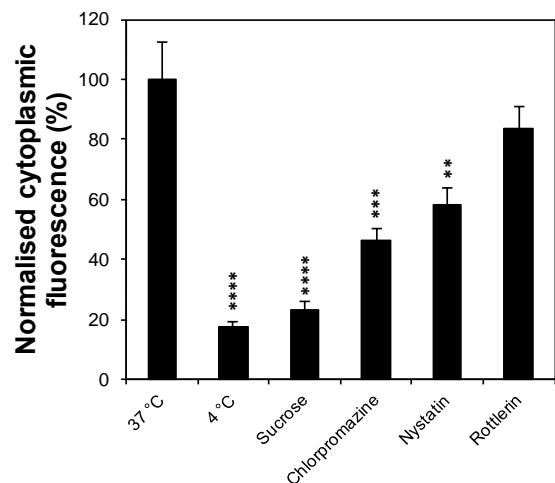


**Figure 6.** Effects of pharmacological endocytosis inhibitors on the uptake of cal@CAU-7, measured by FACS. The statistical significance was determined by using ordinary one-way ANOVA and is indicated in the graph (\*\*P < 0.01, \*\*\*P < 0.001, \*\*\*\*P < 0.0001).

We finally determined the performance and cytotoxicity of CAU-7 loaded with DCA or  $\alpha$ -CHC. **Figure 7** shows the viability of HeLa cells incubated with different concentrations. We used an equivalent amount of CAU-7 for the loaded and empty samples, 0.25, 0.5 and 1 mg/mL, in order to allow a useful comparison. In the case of DCA@CAU-7, cell viability decreased in  $12.5 \pm 8$ ,  $21.9 \pm 5$  and  $26.0 \pm 5\%$  for the tested concentrations, respectively, while free DCA did not have any effects at concentrations below 6 mg/mL (Figure S9a). In the case of the higher loaded amount, it was observed a statistical difference between the DCA loaded MOF and the free molecule. For  $\alpha$ -CHC@CAU-7, the effect was lower than for DCA, with a reduction on cell viability of  $17.0 \pm 8.0$ ,  $6.8 \pm 7.0$  and  $17.2 \pm 8.0\%$ , whereas free  $\alpha$ -CHC did not have any effect up to 1 mg/mL (Figure S9b).

## CONCLUSION

We proposed the use of the bismuth-based MOF CAU-7 for drug delivery applications. We characterized CAU-7 and loaded it with the anticancer drugs DCA and  $\alpha$ -CHC, achieving loadings of 33 and 9 wt.%, respectively. The moderate stability of CAU-7 in the presence of phosphate groups, which can potential prevent its accumulation into cells, combined with an outstanding biocompatibility of the MOF and its building blocks, makes it a promising candidate as DDS. CAU-7 exhibited a progressive release of the drugs, with up to 17 days of release for DCA and 31 days for  $\alpha$ -CHC. Remarkably, after a thermal amorphization process of CAU-7, a 32% slower release of  $\alpha$ -CHC was successfully achieved. We demonstrated that CAU-7 was efficiently internalized by HeLa cells. Since the cellular trafficking of CAU-7 was made partially

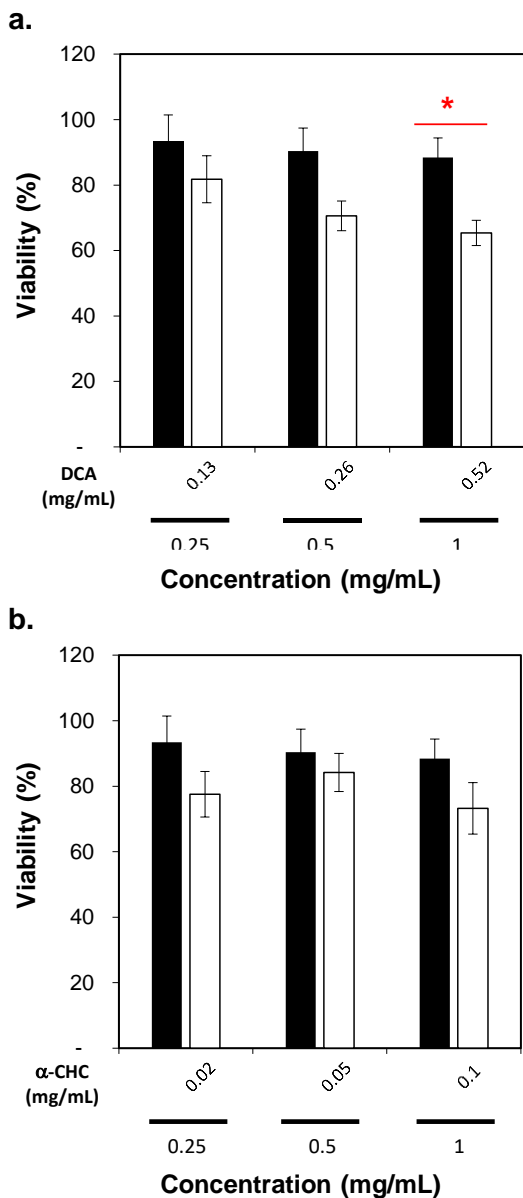


**Figure 7.** MTS assay after 24h of a) DCA@CAU-7, and b)  $\alpha$ -CHC@CAU-7. \* indicates  $P \leq 0.05$  in comparison with the empty MOF (Student's test). Black bars correspond to empty material and white ones to loaded CAU-7.

through caveolae-mediated endocytosis, they can potentially avoid the lysosomes without undermining the therapeutic effect of the DDS, making CAU-7 even more interesting for biomedical applications. All in all, we showed loaded CAU-7 presented an improved performance compared with free drug formulations.

## EXPERIMENTAL SECTION

**Materials:**  $\text{Bi}(\text{NO}_3)_3 \cdot 5\text{H}_2\text{O}$ , DMF and  $\text{H}_3\text{BTB}$  were bought from Alfa Aesar, Grüssing and BASF, respectively. Methanol (99.9%), nystatin, sucrose (99.5 %), rottlerin, sodium dichloroacetate (DCA, 98%) and  $\alpha$ -cyano-4-hydroxycinnamic acid ( $\alpha$ -CHC) were obtained from Sigma-Aldrich (UK). HeLa cells were obtained from the ATCC. Dulbecco's modified Eagle's medium (DMEM), fetal bovine serum (FBS), L-glutamine, penicillin, and

streptomycin were purchased from Invitrogen (UK). Phosphate-Buffered Saline (PBS) and trypsin-EDTA were purchased from Life Technologies™ (UK). The CellTiter 96® Aqueous One Solution Cell Proliferation Assay (MTS) was obtained from Promega (UK). All chemicals and biochemicals used were of analytical grade.

**Instruments:** All PXRD data were collected in Bragg-Brentano geometry on a D8 Bruker diffractometer equipped with a primary Ge monochromator for  $\text{Cu K}\alpha_1$  and a Sol-X solid state detector. Collection conditions were:  $2-50^\circ$  in  $2\theta$ ,  $0.02^\circ$  step size, 15 seconds/step, divergence slits 0.2 mm, receiving slit 0.2 mm. Samples for SEM were scattered onto spectroscopically-pure carbon tabs (TAAB Ltd UK) mounted on aluminium stubs. They were coated with 15 nm of gold in a Quorum Emitech K575X sputter coater to make them electrically conductive. They were imaged in an FEI XL30 FEGSEM, operated at 5 keV, using an Everhart Thornley secondary electron detector. Particle size analysis was determined by dynamic light scattering (DLS) with a Brookhaven Zeta Plus potential analyzer (detection angle of  $90^\circ$  and a 35 mW laser). The measurements were performed in phosphate-buffered saline (PBS) and growth media at room temperature. Thermogravimetric analysis (TGA) was performed using a TA Instruments Q-500 series thermal gravimetric analyzer, with the sample (0.7 - 2 mg) held on a platinum pan under a continuous flow of dry  $\text{N}_2$  gas. TGA curves were obtained using a heating rate of  $5^\circ\text{C}/\text{min}$  and up to  $600^\circ\text{C}$ . The FTIR spectra were recorded in the range  $4000-500\text{ cm}^{-1}$  on an FTIR spectrometer (Perkin Elmer, Spectrum Two).  $\text{N}_2$  sorption isotherms were recorded at 77 K on a BELsorp max. Samples were activated under reduced pressure at  $150^\circ\text{C}$  for 12 h. The BET area was determined using the Rouquerol consistency criteria;<sup>60</sup> the micropore volume was calculated at  $p/p_0 = 0.9$ .

**Synthesis:** In literature, the synthesis conditions of CAU-7 were optimized to form microcrystalline particles.<sup>40</sup> Thus, for medical applications the synthesis conditions were optimised to form nanocrystalline particles. CAU-7 synthesis was carried out under solvothermal conditions in a Biotage Initiator microwave oven. Briefly, 20 mL MeOH were added to a mixture of 1,3,5-benzenetrisbenzoic acid ( $\text{H}_3\text{BTB}$ , 200 mg, 456  $\mu\text{mol}$ ) and ground  $\text{Bi}(\text{NO}_3)_3 \cdot 5\text{H}_2\text{O}$  (148.3 mg, 306  $\mu\text{mol}$ ) in a 30 mL glass vial. The sealed vial was shaken and heated in a microwave assisted synthesis to  $120^\circ\text{C}$  for 20 min under stirring with 900 rpm. The solid product was filtered off and washed with MeOH, DMF and MeOH again. A yellow powder was obtained in a yield of 151.6 mg (52% based on  $\text{H}_3\text{BTB}$ ). The synthesis was repeated 8 times and all products were mixed into one batch after characterization with PXRD. For activation, the sample was heated at  $150^\circ\text{C}$  for 5 h.

**Stability:**  $\text{H}_3\text{BTB}$  release experiments were performed in an incubator at  $37^\circ\text{C}$  with orbital agitation and using phosphate buffered saline (PBS) at pH 7.4 in order to simulate physiological conditions. 5 mg of empty CAU-7 was placed into a dialysis bag (MWCO 3500, molecular weight cut-off Da, Medicell International) with a total volume of 10 mL of PBS. At different times, 1 mL of PBS was taken and replaced with 1 mL of fresh PBS. The amount of linker released was measured by using a UV-vis spectrophotometer at 272 nm. The corrected concentration of  $\text{H}_3\text{BTB}$  release is given by the equation [1]:

$$c_t = c'_t + \frac{V}{V'} \sum_{0}^{t-1} c'_t \quad [1]$$

where  $c_i$  is the corrected H<sub>3</sub>BTB concentration at time  $t$ ,  $c'_i$  is the apparent H<sub>3</sub>BTB concentration,  $v$  is the sample taken and  $V$  is the total volume of the solution. Every experiment was performed by triplicate.

*Drug loading experiments:* DCA adsorption was performed by soaking 250 mg of activated MOF into 5 mL of a methanolic DCA solution (2 M) at room temperature under stirring for 3 days. The  $\alpha$ -CHC loading was achieved by soaking 250 mg of solids in 25 mL of a methanolic  $\alpha$ -CHC solution (10 mg/mL) at room temperature under stirring. In both cases, the loaded CAU-7 samples were collected by centrifugation at 5500 rpm for 20 minutes, washed twice with methanol, centrifuged again for 10 minutes and dried overnight at 80 °C to remove the solvent. The amount of DCA adsorbed was quantified by using oxygen flask combustion technique to burn the samples and collect the chloride present, coming from DCA. The chloride then was titrated in a Radiometer TTT85 auto titrator. The amount of  $\alpha$ -CHC was quantified using TGA measurements.

*Mechanical amorphization:* 0.1 g of drug loaded CAU-7 was placed in a stainless steel jar along with an 8 mm stainless steel ball. The jar was then oscillated at 20 Hz for 30 minutes using a Retsch MM200 mill resulting in amorphous loaded MOF.

*Thermal amorphization:* 40 mg of drug loaded CAU-7 was placed in a glass vial with a small amount of water, enough to get the solids wet. Then, the sample was heated at 180°C for 5 h.

*Delivery:* DCA and  $\alpha$ -CHC release experiments were performed in an incubator at 37 °C with orbital agitation and using PBS at pH 7.4 in order to simulate physiological conditions. 20 mg of DCA loaded CAU-7 or 5 mg of  $\alpha$ -CHC loaded CAU-7 (crystalline, mechanically or thermally amorphous) were placed into a dialysis bag (MWCO 3500, molecular weight cut-off Da, Mediatech International) with a total volume of 10 mL of PBS. At different times, 1 ml of PBS was taken and replaced with 1 ml of fresh PBS. The amount of  $\alpha$ -CHC released was measured by using a UV-vis spectrophotometer at 337 nm. The corrected concentration of  $\alpha$ -CHC release is given by the equation [1]. The amount of DCA released was determined by High Pressure Liquid Chromatography (HPLC). We used a Hewlett Packard 1050 HPLC system supplied with a UV-detector and a SphereClone SAX column (5  $\mu$ m, 4.6x150 mm, Phenomenex). The mobile phase consisted of 10 % Acetonitrile (v/v) and 90 % (v/v) potassium phosphate buffer 200 mM, pH 6.0. The flow rate was set at 1 mL/min and the injection volume was 50  $\mu$ L. The detection of DCA was set at 222 nm and the retention time of DCA was around 1 min. The calibration curve of DCA was prepared in methanol using different concentrations from 0 to 100  $\mu$ g/mL.

*Cell culture:* HeLa cells were maintained at 37 °C with 5% CO<sub>2</sub> in high rich glucose (4500 mg/L) Dulbecco's modified Eagle's Medium (DMEM) supplemented with 10% (v/v) Fetal Bovine Serum (FBS), 2 mM L-glutamine, 100 units/mL penicillin and 100  $\mu$ g/mL streptomycin. The cells were passaged three times a week (at 75-80% of confluence) at a density of  $2.8 \times 10^4$  cells/cm<sup>2</sup>.

*Cytotoxicity assay:* the cytotoxicity activity of DCA and  $\alpha$ -CHC as well as, empty and loaded CAU-7, was investigated using the 3-(4,5-dimethylthiazol-2-yl)-5-(3-carboxymethoxyphenyl)-2-(4-sulfophenyl)-2H-tetrazolium (MTS) (Promega, UK) reduction assay. The day before the experiment, the cells were seeded into a 96-well-plate at a density of  $5 \times 10^3$  cells per well. Prior to the treatments, the cells were washed twice with PBS. The different

amounts of MOF and  $\alpha$ -CHC were dispersed in cell culture media. Then they were added to the cells and incubated for 24 h at 37 °C with 5% CO<sub>2</sub>. To measure the toxicity, the cells were washed extensively to remove the solids, the media was replaced with 100  $\mu$ l of fresh culture media containing 20  $\mu$ l of MTS/phenazine methosulfate (in a proportion 20:1) solution and the plate was incubated for 1 h and 15 min at 37°C with 5% CO<sub>2</sub>. The plates were then read by UV/Vis spectroscopy at 490 nm.

*Confocal microscopy:* HeLa cells were seeded in a NUNC™ imaging four-well-plate at a density of  $1.11 \times 10^5$  cells/mL and incubated for 24 h at 37 °C with 5% CO<sub>2</sub> in DMEM supplemented with 10% (v/v) Fetal Bovine Serum (FBS), 2 mM L-glutamine, 100 units/mL penicillin and 100  $\mu$ g/mL streptomycin. The cells were then washed twice with PBS and incubated together with 0.5 mg/mL of cal@CAU-7 for 24 h. The MOFs were well dispersed in the culture media before being added to the well plates containing the cells. Untreated cells and free calcein (0.056 mg/ml) were included as controls. After the incubation time, cells were washed several times to remove all the non-internalized particles. Cells were then incubated for 15 min with 5  $\mu$ g/ml of Hoechst 33342 (H33342) and 1X of CellMask™ Orange to stain the nucleus and cell membrane, respectively. Cells were then washed extensively to remove the dyes and fresh media without phenol red was added to each sample. Finally, the four-well plate was placed on a Leica TCS SP5 confocal microscope to be imaged. The microscope was equipped with 405 diode, argon and HeNe lasers. Leica LAS AF software was used to analyze the images.

*Flow cytometry assays (FACS):* In FACS experiments, the media of each well was aspirated and the wells were washed extensively. The cells were then harvested by adding 0.1 mL of trypsin and incubated for 5 min at 37 °C with 5 % CO<sub>2</sub>. The cells were recovered by centrifugation, 5 min at 1200 rpm, and re-suspended in 100  $\mu$ l of cDMEM without addition of phenol red. Finally, the samples were measured in a Cytex DxP8 analyzer cytometer within 30 min. The analysis of the data was done using FlowJo and Prism software.

*Treatment with inhibitors:* HeLa cells were seeded in a Cellstar 24-well plate at a density of  $5 \times 10^4$  cells/well and incubated for 48 h at 37 °C with 5 % CO<sub>2</sub> in cDMEM. Then, each well was washed with PBS and pre-treated either at 4 °C or with sucrose (102.7 mg/mL, 0.3 M), chlorpromazine (31.9  $\mu$ g/mL, 100  $\mu$ M), nystatin (250  $\mu$ g/mL), and rottlerin (2.6  $\mu$ g/mL, 5  $\mu$ M) for 30 min at 37 °C. Subsequently, cal@CAU-7 was added and incubated for another 1.5 h., time enough to allow endocytosis processes to take place and avoid the activation of uptake compensatory mechanisms.<sup>36</sup> Subsequently, samples were measured by flow cytometry. The independent values were normalized against the positive control without the addition of inhibitors at 37 °C.

*Computational methods:* We performed grand canonical Monte Carlo (GCMC) simulations of DCA and  $\alpha$ -CHC in CAU-7 at body temperature 310 K with the multi-purpose code RASPA<sup>61</sup> to obtain snapshots of the saturated state of the drugs in CAU-7. The simulations were performed in the NVT ensemble to obtain snapshots of the drugs in CAU-7 at low and medium loadings. We used an atomistic model of CAU-7 for which the framework atoms were kept fixed at the crystallographic positions. We used the standard Lennard-Jones (LJ) 12-6 potential to model the Van der Waals interactions, using Lorentz-Berthelot mixing rules to

define the interactions between the framework and adsorbate atoms, and a Coulomb potential to describe the electrostatic interactions. The parameters for the framework atoms were derived from the Universal Force Field<sup>62</sup> and the Dreiding Force Field,<sup>63</sup> whereas DCA and  $\alpha$ -CHC were modelled with GAFF4RASPA using the general AMBER potential (Table S2).<sup>64</sup> EEq was used to assign the partial charges of the framework. LJ interactions beyond 12.8 Å were neglected. The Ewald sum method was used to compute the electrostatic interactions in the system. Up to 500,000 Monte Carlo cycles were performed, the first 50% of which were used for equilibration, and the remaining steps were used to calculate the ensemble averages. Monte Carlo moves consisted of insertions, deletions, displacements, and rotations. In a cycle, N Monte Carlo moves are attempted, where N is defined as the maximum of 20 or the number of adsorbates in the system.

## ASSOCIATED CONTENT

### Supporting Information

CAU-7 structure, Powder X-Ray Diffraction (PXRD), N<sub>2</sub> Sorption, Scanning electron microscopy (SEM), Stability analysis in PBS and water, PXRD of loaded CAU-7, Thermogravimetric analysis (TGA), Delivery profiles from crystalline and amorphous CAU-7 and, DCA and  $\alpha$ -CHC therapeutic effect evaluation. (PDF). The Supporting Information is available free of charge on the ACS Publications website.

## AUTHOR INFORMATION

### Corresponding Authors

\* E-mails, N.S., [stock@ac.uni-kiel.de](mailto:stock@ac.uni-kiel.de); D.F.-J., [df334@cam.ac.uk](mailto:df334@cam.ac.uk)

### Author Contributions

C. O.-T. and D.F.-J. designed the research. M. K. performed the synthesis and N<sub>2</sub> adsorption under the supervision of N. S. C. O.-T. carried out MOF characterization, drug encapsulation, amorphization, release assays and *in vitro* experiments under the supervision of D. F.-J. A. L. performed the GCMC simulations under the supervision of D. F.-J. The manuscript was written by C. O.-T and D.F.-J. with contribution from all authors. All authors have given approval to the final version of the manuscript.

### Funding Sources

This research was supported by Becas Chile (National Commission for Scientific and Technological Research - CONICYT, Chile) and Cambridge Trust. D.F.-J. thanks the Royal Society for funding through a University Research Fellowship and the European Research Council (ERC) under the European Union's Horizon 2020 research and innovation programme (NanoMOFdeli), ERC-2016-COG 726380.

## ACKNOWLEDGMENT

We thank Prof. Anthony K. Cheetham and Dr. Emma F. Baxter for fruitful discussions about the amorphization of materials. We thank Sanggyu Chong for developing and providing us with GAFF4RASPA, a set of tools for the automatic

generation of input files required for RASPA for the drug molecules DCA and  $\alpha$ -CHC.

## REFERENCES

- (1) Erttmann, R.; Erb, N.; Steinhoff, A.; Landbeck, G. *Cancer Res. Clin. Oncol.* **1988**, *114*, 509–513.
- (2) Meng, L.; Zhang, X.; Lu, Q.; Fei, Z.; Dyson, P. J. *Biomaterials* **2012**, *33*, 1689–1698.
- (3) Shan, K.; Lincoff, a M.; Young, J. B. *Ann. Intern. Med.* **1996**, *125*, 47–58.
- (4) Moghimi, S. M.; Hunter, A. C.; Murray, J. C. *FASEB J.* **2005**, *19*, 311–330.
- (5) Rocca, J. Della; Liu, D.; Lin, W. *Acc. Chem. Res.* **2011**, *44*, 957–968.
- (6) Davis, M. E.; Chen, Z. G.; Shin, D. M. *Nat. Rev. Drug Discov.* **2008**, *7*, 771–782.
- (7) Miller, S. E.; Teplensky, M. H.; Moghadam, P. Z.; Fairen-Jimenez, D. *Interface Focus* **2016**, *6*, 20160027.
- (8) Furukawa, H.; Cordova, K. E.; O’Keeffe, M.; Yaghi, O. M. *Science* **2013**, *341*, 1230444.
- (9) Farha, O.; Eryazici, I.; Jeong, N. C.; Hauser, B.; Wilmer, C.; Sarjeant, A.; Snurr, R.; Nguyen, S. J. *Am. Chem. Soc.* **2012**, *134*, 15016–15021.
- (10) Hönicke, I. M.; Senkovska, I.; Bon, V.; Baburin, I. A.; Bönisch, N.; Raschke, S.; Evans, J. D.; Kaskel, S. *Angew. Chemie - Int. Ed.* **2018**, *57*, 13780–13783.
- (11) Bernini, M. C.; Fairen-Jimenez, D.; Pasinetti, M.; Ramirez-Pastor, A. J.; Snurr, R. Q. *J. Mater. Chem. B* **2014**, *2*, 766–774.
- (12) Horcajada, P.; Gref, R.; Baati, T.; Allan, P. K.; Maurin, G.; Couvreur, P.; Férey, G.; Morris, R. E.; Serre, C. *Chem. Rev.* **2012**, *112*, 1232–1268.
- (13) Deng, H.; Grunder, S.; Cordova, K. E.; Valente, C.; Furukawa, H.; Hmadeh, M.; Gándara, F.; Whalley, A. C.; Liu, Z.; Asahina, S.; Kazumori, H.; O’Keeffe, M.; Terasaki, O.; Stoddart, J. F.; Yaghi, O. M. *Science* **2012**, *336*, 1018–1023.
- (14) Moghadam, P. Z.; Li, A.; Wiggin, S. B.; Tao, A.; Maloney, A. G. P.; Wood, P. A.; Ward, S. C.; Fairen-Jimenez, D. *Chem. Mater.* **2017**, *29*, 2618–2625.
- (15) Köppen, M.; Dhakshinamoorthy, A.; Inge, A. K.; Cheung, O.; Ångström, J.; Mayer, P.; Stock, N. *Eur. J. Inorg. Chem.* **2018**, *2018*, 3496–3503.
- (16) Köppen, M.; Meyer, V.; Ångström, J.; Inge, A. K.; Stock, N. *Cryst. Growth Des.* **2018**, *18*, 4060–4067.
- (17) Inge, A. K.; Köppen, M.; Su, J.; Feyand, M.; Xu, H.; Zou, X.; O’Keeffe, M.; Stock, N. *J. Am. Chem. Soc.* **2016**, *138*, 1970–1976.
- (18) Orellana-Tavra, C.; Haddad, S.; Marshall, R. J.; Abánades Lázaro, I.; Boix, G.; Imaz, I.; Maspoch, D.; Forgan, R. S.; Fairen-Jimenez, D. *ACS Appl. Mater. Interfaces* **2017**, *9*, 35516–35525.
- (19) Orellana-Tavra, C.; Mercado, S. A.; Fairen-Jimenez, D. *Adv. Healthc. Mater.* **2016**, *5*, 2261–2270.
- (20) Horcajada, P.; Chalati, T.; Serre, C.; Gillet, B.; Sebrie, C.; Baati, T.; Eubank, J. F.; Heurtaux, D.; Clayette, P.; Kreuz, C.; Chang, J.-S.; Hwang, Y. K.; Marsaud, V.; Bories, P.-N.; Cynober, L.; Gil, S.; Férey, G.; Couvreur, P.; Gref, R. *Nat. Mater.* **2010**, *9*, 172–178.
- (21) Bellido, E.; Hidalgo, T.; Lozano, M. V.; Guillevic, M.; Simón-Vázquez, R.; Santander-Ortega, M. J.; González-Fernández, Á.; Serre, C.; Alonso, M. J.; Horcajada, P. *Adv. Healthc. Mater.* **2015**, *4*, 1246–1257.
- (22) Agostoni, V.; Horcajada, P.; Noiray, M.; Malanga, M.; Aykaç, A.; Jicsinszky, L.; Vargas-Berenguel, A.

- Semiramoth, N.; Daoud-Mahammed, S.; Nicolas, V.; Martineau, C.; Taulelle, F.; Vigneron, J.; Etcheberry, A.; Serre, C.; Gref, R. *Sci. Rep.* **2015**, *5*, 7925.
- (23) Giménez-Marqués, M.; Hidalgo, T.; Serre, C.; Horcajada, P. *Coord. Chem. Rev.* **2016**, *307*, 342–360.
- (24) Simon-Yarza, M. T.; Baati, T.; Paci, A.; Lesueur, L. L.; Seck, A.; Chiper, M.; Gref, R.; Serre, C.; Couvreur, P.; Horcajada, P. *J. Mater. Chem. B* **2016**, *4*, 585–588.
- (25) McKinlay, A. C.; Xiao, B.; Wragg, D. S.; Wheatley, P. S.; Megson, I. L.; Morris, R. E. *J. Am. Chem. Soc.* **2008**, *130*, 10440–10444.
- (26) Morris, W.; Briley, W. E.; Auyeung, E.; Cabezas, M. D.; Mirkin, C. A. *J. Am. Chem. Soc.* **2014**, *136*, 7261–7264.
- (27) Wang, H.; Chen, Y.; Wang, H.; Liu, X.; Zhou, X.; Wang, F. *Angew. Chemie Int. Ed.* **2019**, *58*, 7380–7384.
- (28) Orellana-Tavra, C.; Baxter, E. F.; Tian, T.; Bennett, T. D.; Slater, N. K. H.; Cheetham, A. K.; Fairen-Jimenez, D. *Chem. Commun.* **2015**, *51*, 13857–13992.
- (29) Teplensky, M. H.; Fantham, M.; Li, P.; Wang, T. C.; Mehta, J. P.; Young, L. J.; Moghadam, P. Z.; Hupp, J. T.; Farha, O. K.; Kaminski, C. F.; Fairen-Jimenez, D. *J. Am. Chem. Soc.* **2017**, *139*, 7522–7532.
- (30) Abanades-Lazaro, I.; Haddad, S.; Sacca, S.; Orellana-Tavra, C.; Fairen-Jimenez, D.; Forgan, R. S. *Chem* **2017**, *2*, 561–578.
- (31) Lim, M. P. A.; Lee, W. L.; Widjaja, E.; Loo, S. C. J. *Biomater. Sci.* **2013**, *1*, 486.
- (32) Huang, H.-H.; He, C.-L.; Wang, H.-S.; Mo, X.-M. *J. Biomed. Mater. Res.* **2009**, *90*, 1243–1251.
- (33) Bertz, A.; Wöhl-Bruhn, S.; Miethe, S.; Tiersch, B.; Koetz, J.; Hust, M.; Bunjes, H.; Menzel, H. J. *Biotechnol.* **2013**, *163*, 243–249.
- (34) Mellman, I. *Annu. Rev. Cell Dev. Biol.* **1996**, *12*, 575–625.
- (35) Rejman, J.; Oberle, V.; Zuhorn, I. S.; Hoekstra, D. *Biochem. J.* **2004**, *377*, 159–169.
- (36) Ivanov, A. I. *Exocytosis and Endocytosis*; John M. Walker, Ed.; Human Press, 2008.
- (37) Guo, C.-J.; Wu, Y.-Y.; Yang, L.-S.; Yang, X.-B.; He, J.; Mi, S.; Jia, K.-T.; Weng, S.-P.; Yu, X.-Q.; He, J.-G. *J. Virol.* **2012**, *86*, 2621–2631.
- (38) Pelkmans, L.; Kartenbeck, J.; Helenius, A. *Nat. Cell Biol.* **2001**, *3*, 473–483.
- (39) Gonzalez-Gaitan, M.; Stenmark, H. *Cell* **2003**, *115*, 513–521.
- (40) Feyand, M.; Mugnaioli, E.; Vermoortele, F.; Bueken, B.; Dieterich, J. M.; Reimer, T.; Kolb, U.; de Vos, D.; Stock, N. *Angew. Chem. Int. Ed. Engl.* **2012**, *51*, 10373–10376.
- (41) Yang, Y.; Ouyang, R.; Xu, L.; Guo, N.; Li, W.; Feng, K.; Ouyang, L.; Yang, Z.; Zhou, S.; Miao, Y. *J. Coord. Chem.* **2015**, *68*, 379–397.
- (42) Wang, Y.; Takki, S.; Cheung, O.; Xu, H.; Wan, W.; Öhrström, L.; Inge, A. K. *Chem. Commun.* **2017**, *53*, 7018–7021.
- (43) Pinheiro, C.; Longatto-Filho, A.; Pereira, S. M. M.; Etlinger, D.; Moreira, M. A. R.; Jubé, L. F.; Queiroz, G. S.; Schmitt, F.; Baltazar, F. *Dis. Markers* **2009**, *26*, 97–103.
- (44) Pinheiro, C.; Longatto-Filho, A.; Azevedo-Silva, J.; Casal, M.; Schmitt, F. C.; Baltazar, F. *J. Bioenerg. Biomembr.* **2012**, *44*, 127–139.
- (45) Pinheiro, C.; Albergaria, A.; Paredes, J.; Sousa, B.; Dufloth, R.; Vieira, D.; Schmitt, F.; Baltazar, F. *Histopathology* **2010**, *56*, 860–867.
- (46) Michelakis, E. D.; Webster, L.; Mackey, J. R. *Br. J. Cancer* **2008**, *99*, 989–994.
- (47) Badr, M. M.; Qinna, N. A.; Qadan, F.; Matalka, K. Z. *Onco. Targets. Ther.* **2014**, *7*, 193–201.
- (48) Ruggieri, V.; Agriesti, F.; Scrima, R.; Laurenzana, I.; Perrone, D.; Tataranni, T.; Mazzoccoli, C.; Lo Muzio, L.; Capitanio, N.; Piccoli, C. *Oncotarget* **2015**, *6*, 1217–1230.
- (49) Amorim, R.; Vilaça, N.; Martinho, O.; Reis, R. M.; Sardo, M.; Rocha, J.; Fonseca, A. M.; Baltazar, F.; Neves, I. C. *J. Phys. Chem. C* **2012**, *116*, 25642–25650.
- (50) Mohan, R. *Nat. Chem.* **2010**, *2*, 336–336.
- (51) Suzuki, H.; Ogawa, T.; Komatsu, N.; Matano, Y.; Murafuji, T.; Ikegami, T. In *Organobismuth Chemistry*; Hitomi Suzuki; Matano, Y., Eds.; Elsevier: Amsterdam, 2001; pp. 21–245.
- (52) Nazareus, M.; Zhang, Q.; Soliman, M. G.; del Pino, P.; Pelaz, B.; Carregal-Romero, S.; Rejman, J.; Rothen-Rutishauser, B.; Clift, M. J. D.; Zellner, R.; Nienhaus, G. U.; Delehanty, J. B.; Medintz, I. L.; Parak, W. J. *Beilstein J. Nanotechnol.* **2014**, *5*, 1477–1490.
- (53) Cunha, D.; Ben Yahia, M.; Hall, S.; Miller, S. R.; Chevreau, H.; Elkaïm, E.; Maurin, G.; Horcajada, P.; Serre, C. *Chem. Mater.* **2013**, *25*, 2767–2776.
- (54) Orellana-Tavra, C.; Marshall, R. J.; Baxter, E. F.; Lázaro, I. A.; Tao, A.; Cheetham, A. K.; Forgan, R. S.; Fairen-Jimenez, D. *J. Mater. Chem. B* **2016**, *4*, 7697–7707.
- (55) Farha, O. K.; Hupp, J. T. *Acc. Chem. Res.* **2010**, *43*, 1166–1175.
- (56) Farha, O. K.; Yazaydin, A. Ö.; Eryazici, I.; Malliakas, C. D.; Hauser, B. G.; Kanatzidis, M. G.; Nguyen, S. T.; Snurr, R. Q.; Hupp, J. T. *Nat. Chem.* **2010**, *2*, 944–948.
- (57) Khormaeae, S.; Choi, Y.; Shen, M. J.; Xu, B.; Wu, H.; Griffiths, G. L.; Chen, R.; Slater, N. K. H.; Park, J. K. *Adv. Funct. Mater.* **2013**, *23*, 1–10.
- (58) dos Santos, T.; Varela, J.; Lynch, I.; Salvati, A.; Dawson, K. a. *PLoS One* **2011**, *6*, e24438.
- (59) Carpentier, J. L.; Sawano, F.; Geiger, D.; Gorden, P.; Perrelet, a; Orci, L. *J. Cell. Physiol.* **1989**, *138*, 519–526.
- (60) Rouquerol, J.; Llewellyn, P.; Rouquerol, F. In *Studies in Surface Science and Catalysis*; 2007; Vol. 160, pp. 49–56.
- (61) Dubbeldam, D.; Calero, S.; Ellis, D. E.; Snurr, R. Q. *Mol. Simul.* **2016**, *42*, 81–101.
- (62) Rappe, A. K.; Casewit, C. J.; Colwell, K. S.; Goddard III, W. a.; Skiff, W. M. *J. Am. Chem. Soc.* **1992**, *114*, 10024–10035.
- (63) Mayo, S. L.; Olafson, B. D.; Goddard, W. A. *J. Phys. Chem.* **1990**, *94*, 8897–8909.
- (64) Wang, J.; Wolf, R. M.; Caldwell, J. W.; Kollman, P. A.; Case, D. A. *J. Comput. Chem.* **2004**, *25*, 1157–1174.

